ASME Journal of Engineering for Gas Turbines and Power
Online journal at:
https://asmedigitalcollection.asme.org/gasturbinespower

On Runway Foreign Object Ingestion With a Variable Pitch Fan in Reverse Thrust Mode

Dimitrios Vitlaris
Rolls-Royce University Technology Centre,
Cranfield University,
Bedford MK43 0AL, UK

David John Rajendran
Rolls-Royce University Technology Centre,
Cranfield University,
Bedford MK43 0AL, UK

Richard Tunstall
Rolls Royce plc,
Bristol BS34 7QE, UK

Barry Moore
Rolls Royce plc,
Bristol BS34 7QE, UK

Rory Clarkson
Rolls Royce plc,
Derby DE24 8BJ, UK

Vassilios Pachidis
Rolls-Royce University Technology Centre,
Cranfield University,
Bedford MK43 0AL, UK

The characterization and quantification of runway foreign object ingestion (FOI) at the end of the landing run with a variable pitch fan (VPF) in reverse thrust mode are described in this work. This is achieved by developing a novel, fully coupled computational fluid dynamics—discrete phase model (CFD-DPM) methodology that allows the tracking of individual debris, which is placed on the runway. The flow field solutions are computed by the three-dimensional (3D) Reynolds-averaged Navier–Stokes (RANS) equations, and the particulate phase is tracked in a Lagrangian way. A modern 300-seater aircraft is considered to feature a high bypass ratio geared turbofan engine architecture on a conventional twin-engine airframe in landing configuration that rolls on the runway at low speeds and a typical high engine power mode. The aerodynamic reverse thrust flow field at such low aircraft speeds is characterized by the development of a "horseshoe" vortex formed in front of the engine that significantly affects the debris trajectories. Based on this, two FOI mechanisms are identified and discussed in detail in the paper. The effect of key debris properties on FOI percentage, such as size, material density, and shape, are investigated and reported. Nonlinear, nonintuitive trends are obtained due to the two-way interaction of flow features and particles. Moreover, a nondimensional analysis that accounts for the changes in debris variables of interest is presented and provides general trends for aircraft with a VPF as the main thrust reversal unit. Generally, debris ingestion increases with lower aircraft speed and debris material density. The benefits of having a VPF are highlighted since it acts as an additional "protective layer" to the engine core and stops and redirects incoming debris from the nominal intake. The assessment of ingestion of foreign objects in realistic end-of-landing-run conditions as described in this study is important to examine the feasibility of reverse thrust-capable VPF engines for future sustainable aircraft.
[DOI: 10.1115/1.4069791]

Keywords: foreign object ingestion, variable pitch fan, reverse thrust

1 Introduction

Future civil turbofan engine development is primarily concentrated on minimizing fuel consumption, which translates to designing engines with lower specific thrust and thus greater propulsive efficiency. To achieve this, the bypass ratio needs to increase, but the fan pressure ratio must decrease to keep the fan power requirement levels reasonable and provide high thermodynamic and overall engine efficiency. However, such low-pressure ratio fans are susceptible to the occurrence of aerodynamic instabilities in off-design conditions. Therefore, a variable pitch fan (VPF) can be utilized to ensure the stable and optimal operation of the fan at different phases of the flight envelope. Previous research studies have indicated that a VPF is the preferred design option and yields improved mission fuel burn by 3%–7% to a variable area nozzle, which would be substantially bulky and heavy due to the greater cold nozzle diameter in these high bypass ratio engines [1–4]. In addition to performance benefits, if the VPF can also be used to generate reverse thrust, the bulky nacelle-based cascade thrust reverser unit can be eliminated from the engine and optimized low installation drag, 'slim-line' nacelles can be implemented, thus making further improvements in fuel burn up to 15% [5]. Therefore, a reverse thrust-capable VPF can significantly contribute to the rapid advancement of fuel-efficient and low-emission, environmentally friendly aircraft, helping the civil aviation industry move closer to achieving NetZero targets [6].

A VPF system follows the concept of a variable-pitch propeller in that the fan blades can rotate. It has been demonstrated that by rotating the fan blade airfoils by around 90 degrees through either clockwise (through feather pitch) or anticlockwise (through flat pitch) rotation, reverse thrust can be achieved as the airflow ingested by the fan stage changes direction and exits through the nominal forward inflow location (see Appendix, Fig. 14). Moreover, the clockwise rotation is the preferable option because it does not

Turbo Expo: Turbomachinery Technical Conference & Exposition (GT2025), June 16–20, 2025. GT2025.
Manuscript received July 30, 2025; final manuscript received September 5, 2025; published online November 12, 2025. Editor: Jerzy T. Sawicki.

Copyright © 2026 by Rolls-Royce plc; reuse license CC-BY 4.0

impose restrictions on blade solidity, as blade entanglement is avoided.

The ability of a reverse thrust-capable VPF was initially explored by NASA in the quiet clean short-haul experimental engine (QCSEE) and the advanced ducted propulsor (ADP) programs [7–10]. These experimental studies were restricted to proving that such designs can establish reverse thrust in an isolated engine at static conditions. Moreover, a low fan pressure ratio and low noise VPF design was developed in the ADP program to fit future high bypass ratio engines. The gap in reverse flow field information in the above studies was addressed by a computational study that investigated the uninstalled reverse thrust flow field of the ADP design at static conditions using 3D RANS simulations [11]. Thereafter, explorations of VPF in reverse thrust were conducted in realistic installed conditions where the reverse flow field was characterized, the core distortion levels and estimated airframe decelerating forces were obtained in a range of aircraft and fan speeds using a computational integrated airframe-engine-VPF model [12–17]. The key outcomes from these studies are that the VPF can generate sufficient reverse thrust of up to 45% MTO to aid aircraft deceleration, and the core operation remains in stable regimes as the circumferential distortion levels are manageable even when the fan transitions from forward flow position to the reverse thrust mode.

When an aircraft is operating on the ground at low speeds with the thrust reversers deployed, there is potential for foreign object ingestion (FOI). The possibility of FOI risk arising depends on numerous parameters, including debris characteristics, engine operating conditions, ambient conditions, and ground clearance. Previous experimental studies that explored debris ingestion using only intakes at close proximity to the ground at static conditions, where the infamous ground vortex is formed, showed that FOI depends on many variables such as particle size and density, intake configuration, and ground surface roughness [18,19]. Moreover, it is widely known that engine components degrade and whole engine operational difficulties may occur as a result of foreign object debris (FOD) ingestion. A report showed that airline operators in 2008 faced costs estimated at $12 billion annually due to FOI issues [20]. The Federal Aviation Administration (FAA) has highlighted the need to build FOI awareness, and various technologies are being developed for FOD detection [21]. Consequently, it is of particular significance to predict and quantify FOD due to ingestion from the runway during the landing run.

Therefore, in this work, FOI scenarios are described and debris ingestion from the runway is quantified using a VPF at the fully reverse thrust mode position at the end of the landing run, where the risk of FOI arises as the aircraft speed is low and the engine power is high. A novel modeling strategy is developed that consists of debris placed on the ground and a fully coupled CFD-DPM approach allowing the two-way interaction of debris and flow features. The effect of key debris properties such as size, density, and irregularity on the levels of FOI is investigated, and general trends are derived using the nondimensional Stokes (St) number. The hitherto unexplored details of a fully deployed VPF operating at low aircraft speeds with runway FOD as attempted in this study, provide insights into FOI risks and highlight the most affected engine components with the VPF being the main thrust reversal unit.

2 Model Description

The potential FOD ingestion mechanisms are investigated using an integrated airframe-engine-VPF model with the VPF set at the fully reverse thrust pitch. This research model was primarily developed to study the feasibility of utilizing VPF for generating reverse thrust, and additional computational capabilities are constantly added to explore further aspects of the reverse thrust-capable VPF behavior. Further details on the model use and VPF investigations on reverse thrust conditions can be found in Refs. [12–16]. The airframe is based on the DLR-F11 and is scaled to accommodate two modern geared turbofan engines, each producing 40,000 lbf of thrust with a 110 in. fan inlet diameter and a bypass ratio of 14 at cruise. The airframe features fully deployed wings, flaps, slats, and spoilers, representing an aircraft in landing configuration. The engine is housed in a short cowl axisymmetric nacelle and is attached to the wing via a typical NACA aerofoil-based pylon design. The internal engine flow path includes a VPF with 18 blade airfoils, a core engine splitter as well as a part of the entry duct into the engine core, an OGV with 40 blade airfoils, a bypass duct, a core exhaust duct, an aft-body casing, and a plug. All components are modeled as full 3D annular geometries to capture flow nonuniformities and track the complete debris paths. The VPF design is based on the 22 in. diameter fan developed in the ADP program and is scaled to the appropriate physical size of 110 in. The flow coefficient and loading distribution remain the same, as well as the tip speed at 245 m/s, but with a modern modified hub-to-tip ratio of 0.3 from 0.42. The VPF blade airfoils are repitched in the fully reverse thrust mode setting, ζ_1 deg, which is a typical reverse flow stagger angle setting that has been characterized by previous studies. The computational domain includes a symmetric half of the airframe with one engine, which is placed in a large cuboidal far-field domain with a rolling runway prescribed at its base by imposing a moving wall boundary condition.

The research aerodynamic model is further developed to include a particulate phase that represents debris and/or small objects. Two thousand particles are introduced uniformly to the domain via a two-dimensional particle injection plane that is placed on top of the rolling runway 2 nacelle lengths ahead of the engine, as shown in Fig. 1. The height of this plane is equal to the particles' diameter and since the fixed frame of reference in the domain is the aircraft, particles follow the same axial direction as the rolling runway and their velocity is equal to the aircraft landing speed. This is analogous to placing debris on the runway. Finally, the centerline of the particle injection plane on the axial axis coincides with the center of the nacelle, and the plane is extended by half a meter on each side of the nacelle.

One of the key challenges during the development of the proposed setup was the additional computational cost that comes from adding a particulate phase to the computations. Thus, to keep the computational budget of the model at reasonable levels without affecting the solution of FOD ingestion, meticulous preliminary analyses were conducted to determine the effect of the location and size of the particle injection plane and the particle number. Different dimensions and particle numbers were tested and optimized based on minimizing the computational cost and their impact on the FOI rate solution. For example, an increase in particle number of more than 2000 makes the model more computationally expensive, but the FOI levels in terms of debris percentage remain the same.

3 Computational Methods

The computational domain is split into main areas: the external to the engine region and the internal engine flow path. A structured mesh is utilized for the turbomachinery components, namely, VPF and OGV, and the core splitter. An unstructured strategy is better suited for the external to the engine region due to the airframe geometry complexity and a total mesh of 50×10^6 elements is finalized after a rigorous GCI study where the grid convergence index was computed to be no more than 0.05 for key local and global

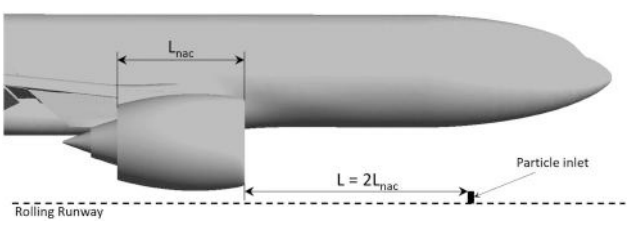

Fig. 1 Schematic of the integrated airframe-engine-VPF model showing the position of particle injection plane

parameters of interest using the Richardson Extrapolation method. The reverse thrust flow field is obtained using 3D RANS solutions and the flow is treated as a compressible ideal gas in a continuum phase. Turbulence closure is achieved by the use of *k*-omega shear stress transport (SST) model [22], and near-wall flow physics is explicitly resolved in regions close to the engine. A fully implicit, commercial, finite volume solver, ANSYS-CFX, is used to solve the equations with second-order accurate spatial discretization schemes. Convergence has been reached typically after 1500 iterations while the solution is considered converged when a) the maximum imbalance of the linearized transport equations in each domain drops below 0.001% and b) the value at the current iteration of key parameters, such as Mach numbers, forces and mass flow rates, is within 0.5% compared to the mean of the last 25 iterations.

4 Debris Tracking Method

The particulate phase is modeled utilizing a discrete particle transport approach. In detail, each particle is tracked over time along its trajectory through the continuum fluid in a Lagrangian way. Because the concentration of particles is small enough in the flow field and the aim of this work is the investigation of potential FOD ingestion from the runway due to engine suction, particle–particle interactions, and collisions are neglected. Moreover, the buoyancy force, the pressure gradient force, the added mass force, and the Basset history force are neglected because the difference between the density of the fluid and solid particles is large and the freestream velocity is relatively high [23]. Based on these assumptions, the equations of motion for the particles are as follows:

$$x_p^n = x_p^0 + \mathbf{U}_p^n dt \tag{1}$$

$$m\frac{d\mathbf{U}_p}{dt} = F_D + F_R \tag{2}$$

where n and 0 is the new and old position of the particle, respectively, $\mathbf{U}_p$ is the particle velocity, dt is the time-step, F_D is the drag force and F_R is the force due to domain rotation, i.e., centripetal and Coriolis forces, and is taken into account only for the fan domain.

In this work, the Lagrangian framework is fully coupled with the CFD modeling. The flow field affects the particle trajectories, while the particles, in turn, impact the fluid behavior. This interaction is defined as a two-way coupling approach. For that reason, particle source terms, which are generated for each particle as it travels in the flow, are added to the fluid momentum equations.

4.1 Effect of Particle Irregularity. The effect of drag coefficient on FOD ingestion is also investigated in this study. The drag coefficient for the perfect spherical particles is calculated using the well-established Schiller and Naumann model [24], which relates the particle drag coefficient to its Reynolds number as follows:

$$\begin{cases} \dfrac{24}{\mathrm{Re}_p}\left(1 + 0.15\mathrm{Re}_p^{0.687}\right) & \mathrm{Re}_p \le 10^3 \\ 0.44 & \mathrm{Re}_p > 10^3 \end{cases} \tag{3}$$

However, all sorts of debris shapes can be found on the runway ranging from perfect spheres to nonspherical particles with irregular, angular shapes. The drag force is the main parameter that influences the behavior of such particles suspended in a flow. Irregular particle geometry can cause drag forces to be an order of magnitude different from that of spherical particles of equivalent volume [25]. To account for the difference in particle shape, the drag coefficient of such particles changes according to shape factors. The shape factors considered in this work are computed based on a specific formula derived using sand particles in experiments

$$C_{\text{shape}} = \frac{C_{D,\text{shape}}}{C_{D,\text{shpere}}} \tag{4}$$

$$C_{\text{shape}}^2 = 1 + 1.5(A_{\text{surf}}^* - 1)^{1/2} + 6.7(A_{\text{surf}}^* - 1) \tag{5}$$

where C_{shape} is the shape factor, A_{surf}^* is the ratio of the surface areas of nonspherical particles to perfect spheres. A_{surf} is obtained using empirical relations from experiments and 2 values are chosen, one for particles of an ellipsoid shape and another for irregular particles. Based on these, two shape factors are computed: 1.7 and 2.3. These factors are then multiplied by the drag coefficient of spherical particles. Therefore, when the Re_p is higher than 1000, the drag coefficient of the ellipsoid particles is $0.44 \times 1.7 = 0.75$, and for angular particles, it is computed as $0.44 \times 2.3 = 1.012$.

4.2 Foreign Object Ingestion Validation. The methodology that enables FOD ingestion from the runway is validated using available experimental data from a static case that tested the ingestion thresholds of debris during ground running by a ducted intake [18]. The lack of experimental and computational public data on debris ingestion when the aircraft operates at the end of the landing run with deployed thrust reversers led to the selection of this study which investigated debris ingestion at static conditions due to the formation of ground vortex. The vortical flow field is characterized by steep pressure gradients with a reduction in static pressure at the vortex core that affects the pressure close to the ground. Therefore, the particles on the ground are exposed to local pressure variations as well as the velocity field that is generated by the vortex.

The test rig setup is seen in Fig. 2(*a*) and glass balls are placed on the ground below the intake along with the obtained computational results. Tests were conducted at different crosswind and intake velocities, and different ball diameters were used. This experimental campaign provided the ingestion threshold based on the intake diameter and the ratio of intake to crosswind velocity, and is used as a computational validation metric. The ingestion points predicted by the model, as seen in Fig. 2(*b*), are in strong agreement with the experimentally derived ingestion threshold. Therefore, this study concludes that the current particle tracking approach provides great accuracy for FOD ingestion investigations in the presence of pressure gradients in a flow field.

5 Boundary Conditions

The likelihood of FOD ingestion arises at the end of the landing run, when the thrust reversers are deployed, the engine's power is relatively high, and the aircraft has low speed. Therefore, the VPF is at the fully reverse thrust mode setting of ζ_1^0 and the engine is set at a typical value of 80% of the fan design speed (N_1). Three different aircraft landing speeds of 40, 50, and 60 knots are considered, which

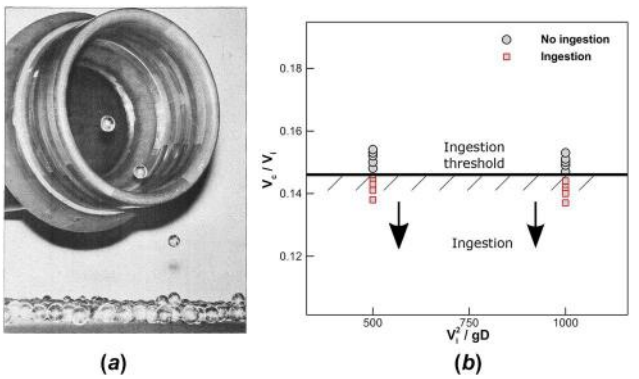

Fig. 2 Numerical model validation: (*a*) experiment test showing ingestion [18] and (*b*) Ingestion prediction by the numerical model agreeing well with the experimental results

Table 1 Solution matrix showing all investigated conditions in this paper

Parameter	Condition		
Aircraft speed	40	50	60
Fan stagger angle	Reverse thrust pitch (ζ_1°)		
Fan rotational speed (% of maximum rpm)	80%		
Particle density (kg/m^3)	1650	2500	3500
Particle diameter (mm)	0.1 and 1		
Particle shape factors ($C_{D,\text{shape}}$)	1	1.7	2.3

represent typical minimum aircraft velocities—well known to pilots—before the thrust reverser mechanism is retracted. Furthermore, ISA, SL conditions with an atmospheric pressure and a temperature of 288.15 [K] are specified for the far field. The core engine modeling is carried out explicitly by an engine thermodynamic model built in NPSS. This model provides the engine conditions at the core entry duct and core exhaust nozzle and ensures that the engine performance is completely aligned with the integrated model. Finally, FOI mechanisms are investigated and the effect of key debris properties such as size, density, and shape on FOI rate is explored. Two particle sizes of 1 mm and 0.1 mm are considered, three particle densities representative of runway debris are utilized ($\rho = (1650\,\text{kg/m}^3, 2500\,\text{kg/m}^3, 3500\,\text{kg/m}^3)$) and three different particle shapes ranging from perfect spheres to highly irregular shapes are examined leading to a matrix of 54 simulations. Table 1 shows the entire solution matrix and the conditions studied for FOI investigations.

6 Results and Discussion

To fully characterize and quantify FOI mechanisms with the VPF at the reverse thrust setting at the end of the landing run, the results are presented in the following order:

(1) First, the installed aerodynamic reverse thrust flow field is briefly described for three aircraft landing speeds of 40, 50, and 60 knots and a fan rotational speed of 80% N_1. The development of specific flow features and their effect on potential FOD ingestion are highlighted.
(2) The effect of particle size on FOI is obtained and discussed for the three aircraft speeds and constant particle density and shape of $\rho = 1650(\text{kg/m}^3)$ and $C_{D,\text{shape}} = 1$ respectively. FOI processes are completely characterized and FOD ingestion is quantified. Even though investigations were undertaken for 10 mm diameter particles, no FOI scenarios were identified. Therefore, this work only presents cases where FOD ingestion is observed and considers particles of 0.1 mm and 1 mm diameter.
(3) The ingestion percentage and process are certainly affected by the particles' density. Therefore, the effect of three particle densities of $\rho = [1650, 2500, 3500](\text{kg/m}^3)$ is described at the three aircraft speeds and at constant particle diameter of 0.1 mm and shape of $C_{D,\text{shape}} = 1$. The selected values are representative of runway debris with the two lower ones representing low- and high-concentration sand suspended in the flow while light metal particles are defined by the highest density.
(4) The effect of particle shape is also investigated to determine the behavior of irregular debris on FOI percentage for the three aircraft speeds. Three shape factors of $C_{D,\text{shape}} = [1, 1.7, 2.3]$ are utilized while the other particle properties remain constant at $\rho = 1650(\text{kg/m}^3)$ and 0.1 mm diameter.
(5) Finally, a parametric analysis is conducted for all investigated particle parameters and the various results are presented in a concise manner using a nondimensional parameter to provide general trends of FOI rates.

6.1 Installed Reverse Thrust Flow Field at Low Aircraft Speeds. Figure 3 shows the reverse thrust flow field internal and external to the engine for three aircraft speeds using 2D streamlines colored by axial velocity in a meridional midengine plane. In all aircraft speeds, when the VPF is deployed at the reverse thrust pitch, the fan suction acts in the nominal fan outlet and bypass regions. This causes the engine to ingest flow from the bypass nozzle exit that travels inside the bypass duct toward the fan stage and intake. The reverse stream passes through the OGV blade row, and a portion of the reverse stream turns abruptly and feeds the core engine, forming separation zones close to the splitter edge. The remaining portion is directed to the fan stage where it enters the fan passages and meets the freestream, which penetrates the fan from the intake. The two streams mix and form a shear layer inside the fan passages and are centrifuged radially outward. As they reach the fan shroud regions, a

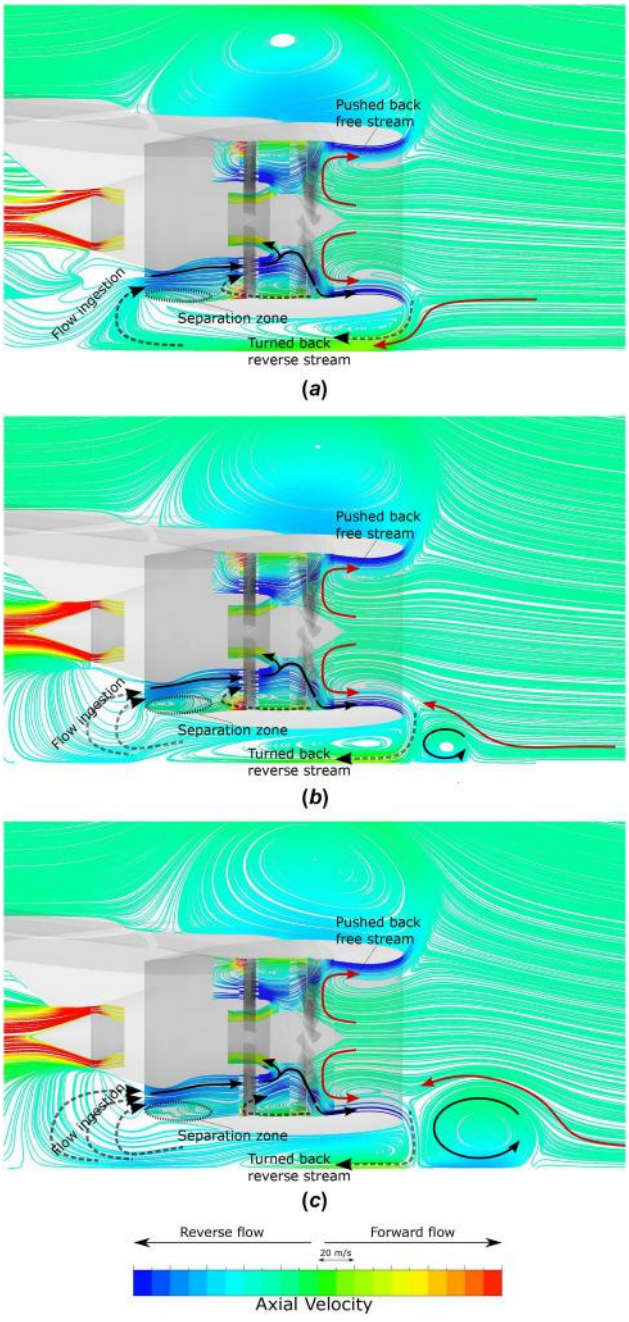

Fig. 3 Aerodynamic flow field with the VPF at the reverse thrust mode position at three different aircraft speeds: (*a*) 60 knots, (*b*) 50 knots, and (*c*) 40 knots

part of this flow turns back toward the bypass nozzle exit, interacts with the OGV blades, which makes it lose momentum, and rejoins the reverse stream that is ingested from the bypass nozzle exit. The other part leaves the engine from the intake at higher spanwise locations. It is highlighted that the freestream that comes into the engine from the intake is pushed back by the generated reverse stream in the fan stage. The developed flow features inside the engine are very similar for all three aircraft landing speeds with small differences noticed in their velocity magnitude and topology.

In regions that are external to the engine, flow that emanates from locations close to the ground is ingested from the bypass nozzle exit. As described above, this happens because of the VPF suction that acts on the rear of the engine. The ingested reverse stream travels inside the engine and a portion of it is injected out of the fan inlet with a swirl angle due to the fan rotation. After the reverse stream reaches the nacelle lip, it leaves the engine and expands in outer regions forming large recirculation zones around the nacelle. These zones occur because the freestream momentum at such aircraft speeds is low enough that the interaction with the dominant reverse stream leads to these large separation areas. The engine's proximity to the ground creates a ground effect and causes differences in the development of the external flow field for the three aircraft speeds. As the aircraft speed decreases, the freestream momentum reduces making the reverse stream more powerful. At 50 knots, an additional recirculation region, which was not present at 60 knots, appears in front of the nacelle inlet as a result of the predominant reverse stream occupying most of the volume between the engine and the ground. This forces the freestream to create a recirculation zone in the opposite direction due to the restricted space for mixing. At 40 knots, this recirculation region has grown more due to the lower freestream velocity and occupies a larger volume in front of the intake. The higher negative axial velocity close to the ground of this zone stems from the reverse stream and also contributes to its greater volume and strength. Finally, these recirculation zones form a three-dimensional "horseshoe" vortex around the engine with the same size as the zones seen at 40 and 50 knots. The formation of this "horseshoe" vortex is a unique flow feature only to engines with a reverse thrust-capable VPF and plays a crucial role to the debris trajectories inside and outside the engine.

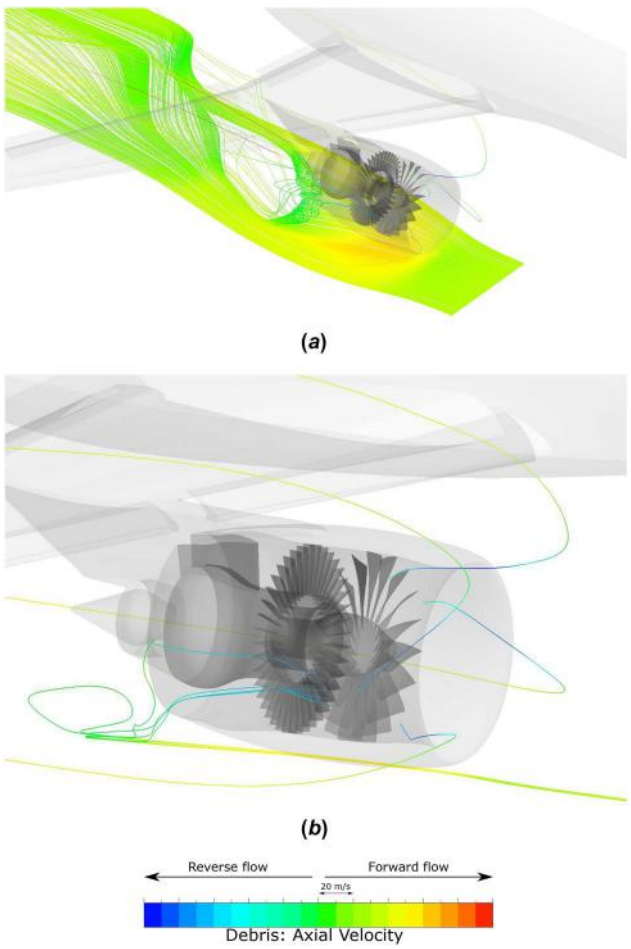

Fig. 4 Debris trajectories of 0.1 mm diameter particles at 60 knots aircraft speed

6.2 Effect of Particle Size. The effect of particle size on FOI is described in this section for the three aircraft landing speeds using spherical particles of constant density. Starting from the highest landing speed, Fig. 4 shows the trajectories of the smallest particles highlighted by particle axial velocity. At this aircraft speed, only particles of 0.1 mm diameter are ingested. Initially, due to the ground effect, particles gain momentum below the nacelle, but a few of them are picked up just behind the bypass nozzle exit. This happens because the engine's suction is greater than the gravitational force of individual particles. Figure 4(*b*) shows the trajectories of the particles that are ingested into the engine. Here, the first FOI mechanism is identified, where 0.4% of all particles go into the engine from the bypass nozzle exit. These particles follow the direction of the reverse stream inside the bypass duct, interact with specific OGV blades, and their trajectory changes marginally. Then, they enter the fan rotor domain and leave it from the fan inlet moving toward the nacelle inlet. Inside the fan passages, they gain a radial velocity component following closely the reverse stream, while the interaction with the fan blades and fan rotation causes them to scatter until they are eventually pushed out of the engine from higher spanwise locations. It is worth noting that none of the ingested particles go into the engine core in this analysis, even though a portion of the reverse stream feeds the core.

The second FOI mechanism is observed in Fig. 5, which shows the trajectories of 0.1 mm diameter particle at 50 knots. The effect of the additional recirculation region that forms in front of the nacelle is noticed as most of the particles are trapped within the vortex and travel along with it and around the engine. Some particles manage to leave the recirculation zone because of their higher inertia and end up inside the engine from the intake. The ingested particles, which account for 0.5% of all particles, interact with the fan blades, and all of them are pushed back out of the nacelle inlet by the reverse stream. Due to the developed reverse stream in the fan stage and the physical obstruction of VPF blades, none of these particles pass the fan stage, and all of them leave the engine from the outer annular regions. It is calculated that once again, the trajectories of the particles are significantly affected by the interaction with the VPF blades, and they disperse after moving out of the engine intake. In this aspect, the VPF plays a crucial role in the integrity of the core engine and provides an extra protective layer from potential FOD ingestion to turbomachinery component damage.

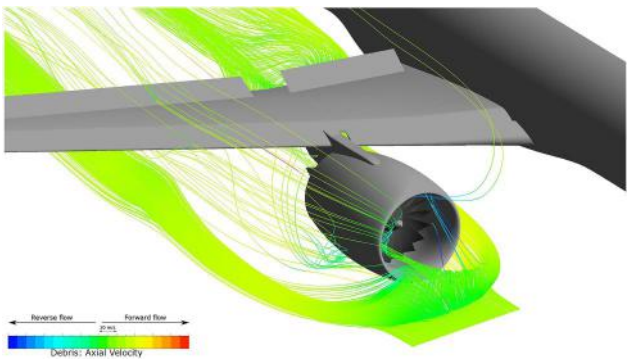

Fig. 5 Debris trajectories of 0.1 mm diameter particles at 50 knots aircraft speed

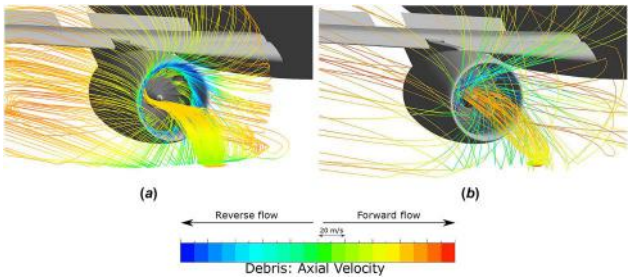

Fig. 6 Debris trajectories at 40 knots aircraft speed: (*a*) 0.1 mm diameter and (*b*) 1 mm diameter

As the aircraft speed drops to 40 knots, the same FOI mechanism as the 50 knots case applies but the main difference is the "horseshoe" vortex size and strength that has a significant impact on particle trajectories, as seen in Fig. 6. It is observed that FOD ingestion occurs for both particle sizes, and more particles are directed into the engine from the intake at 50 knots aircraft speed. This vortex has a stronger influence on particle behavior and manages to lift heavier particles, leading them inside the engine. Moreover, the ingested particles travel inside the fan stage from the inner annular regions. This happens because the vortex entraps the particles and moves them to higher positions from the ground, and the particles that manage to escape it follow the penetrated freestream into the engine toward the fan blades. 9% and 3.6% of all particles go into the engine for the 0.1 mm and 1 mm particle diameters, respectively. The reverse stream collects the incoming debris and forces it out of the engine from the intake, protecting the engine components downstream once more.

6.3 Effect of Particle Density. This section explains the effect of particle density on FOI scenarios for the three different aircraft speeds using spherical particles of 0.1 mm diameter. Figure 7 shows the percentage of ingested particles based on the particle's density, and each line represents a constant aircraft speed. As the density increases, the only affected property is the particle's weight and thus, its inertia, which increase too. The remaining forces, drag and lift, are unchanged because the related parameters are kept the same. At 40 and 60 knots, a pattern emerges in which fewer particles are ingested with an increase in particle density. At 60 knots, specifically, there is no particle ingestion for the two largest density values. This happens because the particles with higher inertia are affected less by the flow field. With an increase in density at 40 knots, a small drop in FOI is initially noticed for particles with 2500 kg/m^3, while a slight increase in ingested particles with a further increase in density is obtained. The small differences in this case are explained by the vortex formation and strength as it manages to lift up particles, and approximately the same amount of particles escape from it in all different density cases.

This trend is not observed for the aircraft speed of 50 knots. In this condition, more particles are ingested with an increase in particle density. The difference in FOI percentage is highlighted in Fig. 8, which shows the ingested particle trajectories for the three different particle densities. Here, the vortex is strong enough to pick up particles but entraps fewer particles with higher densities because of their larger inertia. The escaped particles are then directed into the engine following the freestream path, leading to higher FOI rates.

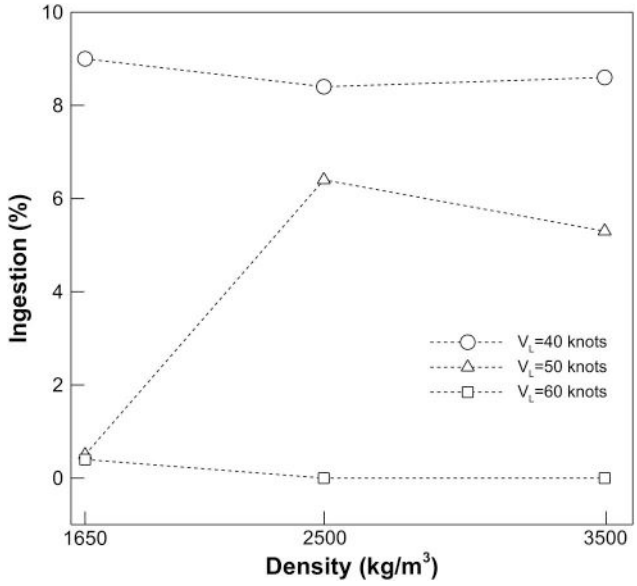

Fig. 7 Effect of particle density on FOD ingestion using spherical particles of 0.1 mm diameter for three aircraft speeds

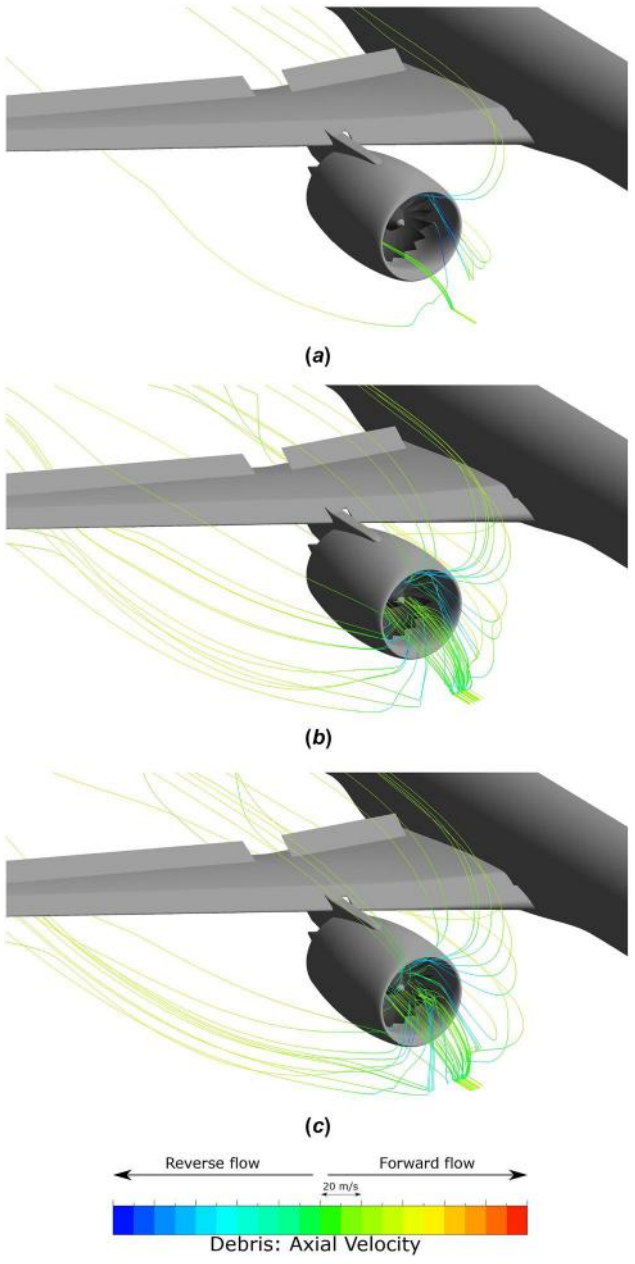

Fig. 8 Ingested debris trajectories of 0.1 mm diameter at 50 knots aircraft speed: (*a*) $\rho = 1650$ kg/m

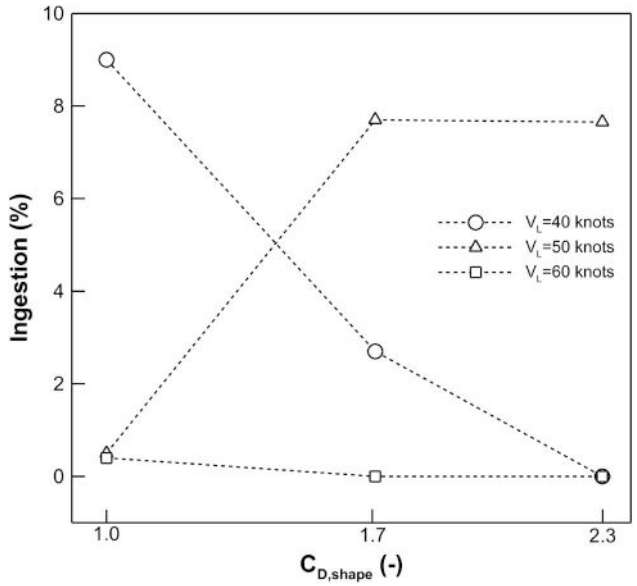

Fig. 9 Effect of particle irregularity on FOD ingestion using particles of 0.1 mm diameter and 1650 kg/m

The effect of particle density on FOI percentage shows the influence of particle inertia and produces nonlinear, possibly nonintuitive relationships. The vortex size and strength in front of the engine affect the trajectory of heavier particles and play an important role in FOI levels.

6.4 Effect of Particle Irregularity. The effect of particle shape on FOI scenarios for the three different aircraft speeds using particles of 0.1 mm diameter and 1650 kg/m^3 density is described in this section. The shape of a particle is directly linked to its drag and $C_{D,\text{shape}}$ factors derived from experiments are utilized and multiplied to the particle C_D. The higher the drag coefficient, the more irregular the particle is, and therefore, more drag is induced. This means that the resistance of the particles to flow changes is higher, thus, they follow the flow more closely.

Figure 9 shows the percentage of ingested particles based on particle's drag coefficient while each line represents a constant aircraft speed. A decreasing trend of particle ingestion is noticed at the aircraft speeds of 40 and 60 knots. The FOI mechanism at 60 knots is characterized by particles that go into the engine from the bypass exit. The engine's suction at the rear has a lower effect on particles with higher C_D and therefore, the FOI percentage decreases. At 40 knots, the large recirculation zone in front of the engine entraps more and more particles as the C_D increases, where eventually all particles are trapped inside the vortex at $C_{D,\text{shape}} = 2.3$ and travel along its way and around the engine. At 50 knots, the FOI percentage increases with an increase in $C_{D,\text{shape}}$, which indicates a change in the flow field.

Figure 10 shows the flow field containing the particles (left) at 50 knots using flow streamlines colored by axial velocity and particle trajectories (right) for the three different values of particle $C_{D,\text{shape}}$. As the C_D increases, the vortex shape and position change, and it moves closer to the engine and the nacelle intake lip. The change in flow topology occurs due to the higher C_D of the particles that are concentrated in that region. The vortex picks up the resisting particles and entraps them leading to an increase in its overall drag, making it move closer to the engine. Additionally, particles with higher C_D resist the movement of the recirculation zone and are concentrated in outer recirculation areas away from the vortex core. This causes a change in the vortex shape and specifically, the recirculation zone moves at higher locations reaching areas above the nacelle intake lip. This change plays a critical role in particle trajectory because as soon as particles that are carried along the vortex reach regions above the nacelle lip, more of them escape the recirculation zone and follow the freestream into the engine, since the recirculatory flow direction changes abruptly due to the obstruction of the nacelle lip. This explains why the FOI levels are higher at the aircraft speed of 50 knots. Approximately 8% of all particles are ingested into the engine for the highest two $C_{D,\text{shape}}$ values as the flow topology remains the same.

This condition highlights the influence of the particulate phase on the flow field. The interaction of the flow and particles is enabled only by a coupled CFD-DPM framework as used in this work. In such cases where there is a noticeable difference in the development of flow field, decoupled methods lose important information and therefore are not suitable for such analyses.

6.5 General Trends on Foreign Object Ingestion Percentage. The influence of a single particle property parameter on the particle behavior and in terms of FOI percentage is explained in previous sections. This section describes an extensive parametric analysis to determine how individual parameters, as well as combinations of them, affect FOI levels. This is done to identify general FOI trends for engines, of which the main thrust reversal unit is a VPF. The parameters considered in this study are the particle diameter, density, shape, and aircraft landing speed. Therefore, a large matrix of 54 simulations is generated by combining all possible scenarios.

A global parameter that incorporates the variables under investigation must be chosen to extract FOI patterns and present the results succinctly. For that reason, the effect of each individual variable in the forces acting on the particles needs to be explained. Figure 11 shows a simple schematic of the forces acting on each particle in this study. The particle motion is affected by three main forces: the gravitational force, which comes from the weight of the particle, and the resultant aerodynamic force, which is further divided into two forces, drag and lift. Starting from the particle density, only the particles' weight, and thus the gravitational force, is affected by changing this variable. Accordingly, only the particles' drag changes when the particle $C_{D,\text{shape}}$ varies. However, the particle diameter affects all forces since with higher values, the particle weight increases as well as its area, which affects the aerodynamic forces. Therefore, the final combined parameter must include all these effects. Additionally, it has to include the effect of the aircraft speed, which is directly correlated to the dynamic head of the freestream, as it plays an important role in flow field development.

Based on the above analysis, preliminary studies, in which a wide range of potential global parameters was explored, concluded that the particle behavior can be characterized using the dimensionless Stokes number for all investigated variables. Generally, this number is used to predict the behavior of particles suspended in a fluid flow. High Stokes number values indicate that the particle will be less affected by the flow changes, while low values show that the particle will follow the flow closely. The Stokes number is defined as

$$S_t = \frac{\rho_p U_\infty d_p^2}{18 \mu_f l_c} \tag{6}$$

where ρ_p is the particle density, d_p is the particle diameter, U_∞ is the freestream velocity, μ_f is the viscosity of the fluid and l_c is a characteristic length which is defined as the length of the particle injection inlet.

Figure 12 shows the Stokes number of all investigated scenarios where ingestion occurs and their FOI percentage levels. The plot is characterized by the identification of two groups of points. The first one is formed at low Stokes numbers and includes only the particles of 0.1 mm diameter, while the other group consists of the bigger particles. The particle diameter is the most influential parameter in this plot and it divides the analysis into two categories based on particle size. FOI trends are first obtained in the group of 1 mm

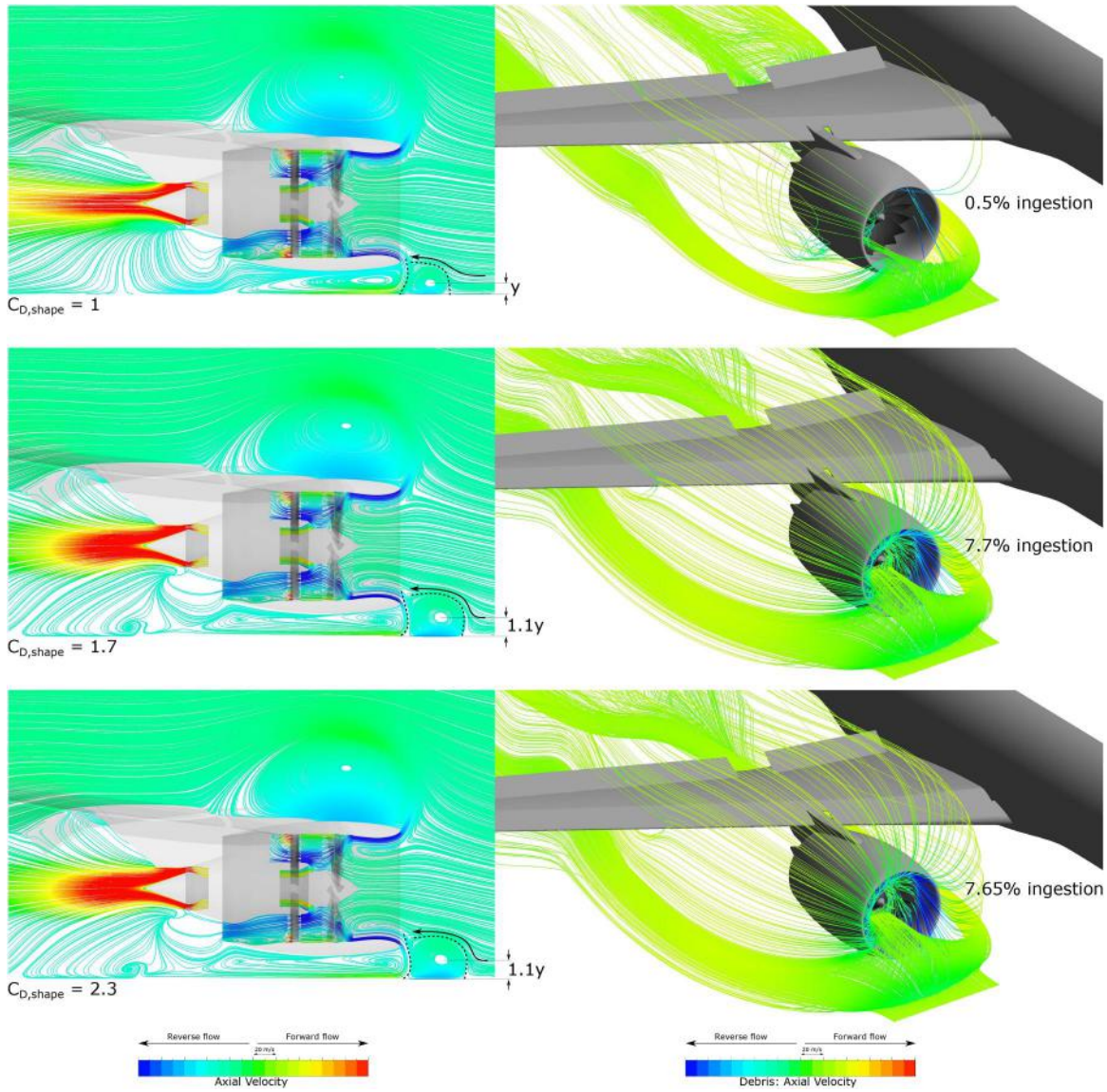

Fig. 10 Two-dimensional flow streamlines (left column) of coupled CFD-DPM results for different $C_{D,\text{shape}}$ values and debris trajectories (right column) at 50 knots

diameter particle based on the Stokes number. Particles of such size are ingested only at 40 knots of aircraft speed. As the particle density increases for the same irregular particles—$C_{D,\text{shape}}$ factors remain the same—fewer particles are ingested. Therefore, the FOI percentage decreases as the particle density and Stokes number increase. The relationship is almost linear in the lowest and highest $C_{D,\text{shape}}$ values, while a sharper decrease in FOI percentage is noticed at $C_{D,\text{shape}} = 1.7$. Moreover, an increase in irregularity for particles of the same density causes an increase in FOI percentage. The two highest particle diameter cases provide similar behavior, as the FOI

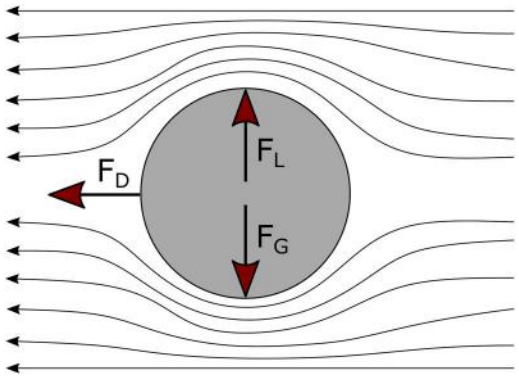

Fig. 11 Schematics of forces acting on a particle

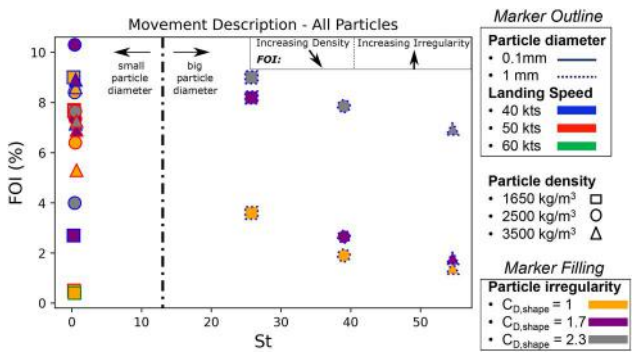

Fig. 12 FOD ingestion based on Stokes number. General trends are indicated for particles of 1 mm diameter at the top right corner.

increase is small from $C_{D,\text{shape}} = 1$ to $C_{D,\text{shape}} = 1.7$ and becomes greater moving to the highest $C_{D,\text{shape}}$. The general trends are indicated by two arrows showing the effect of variables on FOI percentage in the top right corner of the plot. Finally, the Stokes number is the same for particles with equal density because the aircraft landing speed remains at 40 knots.

Figure 13 shows the FOI percentage for the group of 0.1 mm particle in two plots. Such particles are ingested at all three landing speeds. Only one ingestion scenario is noticed at 60 knots, which is the one seen in Fig. 4, where 0.4% of particles go into the engine. The plot is split into three specific portions (colored sections) based on particle density. This division shows trends of expected FOI levels based on particle density for a range of Stokes numbers. The boundaries of the sections are derived using a linear relationship between particles that are located at the limits. The effect of aircraft speed is noticed in every colored portion since ingested particles at higher aircraft speeds have a higher Stokes number. In detail, two subgroups are noticed in all three portions: a subgroup in which the ingested particles at the lowest landing speed have low Stokes number and another subgroup where the particles have high Stokes number, thus ingested at higher landing speed. In the latter subgroup, the FOI percentage increases with the particle irregularity, agreeing with the conclusion drawn for particles of 1 mm diameter. This behavior is noticed at 50 knots and for $\text{St} = (0.32, 0.49, 0.69)$. This trend is not noticed at 40 knots landing speed because of the change in flow topology. To conclude, even though the influence of particle density is not as strong as the particle diameter, the Stokes number changes, and based on this variable, three distinguished portions are derived that provide guidelines on FOI levels based on debris density.

Another FOI trend is noticed for the ingested particles at 40 knots aircraft speed. For such particles, an increasing FOI behavior is obtained as the Stokes number increases. Therefore, a linear threshold line is determined (blue dashed line) below which no ingestion occurs. The same analysis can be applied to the ingested particles at 50 knots aircraft speed. With the exemption of one case, particles of $\rho = 1650\,\text{kg/m}^3$ and $C_{D,\text{shape}} = 1$, threshold lines (red dashed lines) are drawn to highlight the expected FOI percentages. At this landing speed, the points in the plot are getting more scattered as the Stokes number increases, but the FOI percentage remains at similar levels of around 7%.

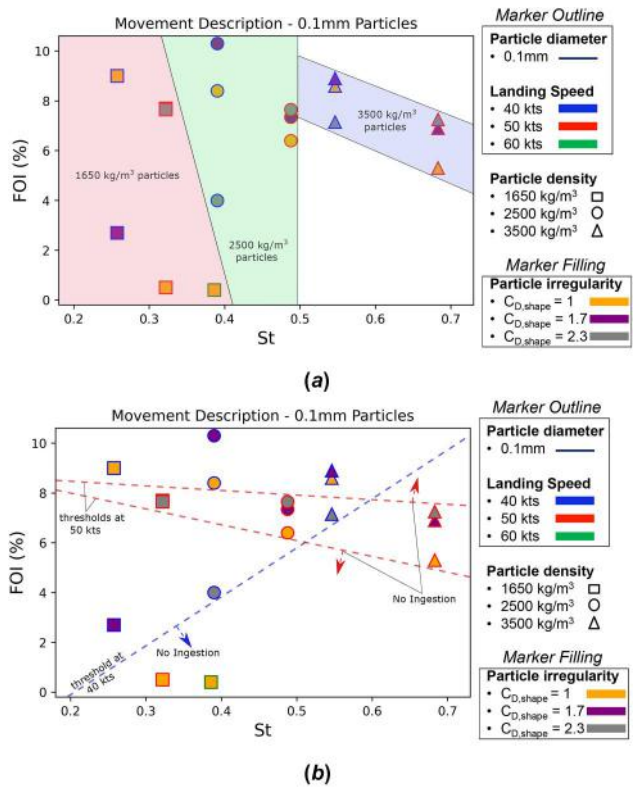

Fig. 13 FOD ingestion based on Stokes number for the smaller particles. General trends are identified based on particle density (*a*) and aircraft speed (*b*).

The above analysis explains the behavior of particles for multiple particle parameters on FOI percentages using only one dimensionless variable. General FOI trends are determined that show FOI percentages based on Stokes number for a specific parameter. Simple linear approximations are derived based on the simulation matrix while more simulations are required for the increased fidelity of these trends. The outcomes of this analysis are the following:

- The regime that includes high Stokes numbers contains the biggest particles in size. In this region, the trends are well-defined because particles are ingested only at 40 knots of aircraft speed. Specifically, FOI percentages increase with an increase in particle irregularity and a decrease in particle density.
- Particles of smaller sizes are noticed in regimes defined by low Stokes numbers. The general trends in this case may be indistinct initially because particles are ingested at all three aircraft landing speeds. However, FOI levels can be determined by using the particle density parameter, which divides the Stokes plot into three discrete portions. Additionally, the aircraft landing speed parameter provides boundaries of expected lower and upper FOI percentage limits.

7 Conclusion

The likelihood of FOI in the engine when the VPF operates in reverse thrust pitch and low aircraft speeds is analyzed using a novel fully coupled CFD-DPM approach, where debris is placed on the runway. An extensive sensitivity study has been conducted using a matrix of 54 simulations based on different particle diameters, densities, and shapes at three low aircraft landing speeds. Consequently, the effects of particle diameter, density, and irregularity on particle ingestion have been investigated for all three landing speeds. A horseshoe vortex is formed in front of the engine at the lower two aircraft speeds and plays a critical role in the behavior of particles. Additionally, the dimensionless Stokes number is used to identify general trends to indicate potential FOI levels for cases beyond the investigated ones in this study. Therefore, the key observations are:

- Two FOI mechanisms are identified where particles/debris are ingested into the engine. The first one is characterized by particles being ingested from the bypass nozzle exit and occurs at 60 knots of aircraft speed. The second includes particles going into the engine from the nacelle intake, where they interact with the VPF blades. In both scenarios, all simulations show that the particles are directed out of the engine due to the reverse stream, and none of them are ingested into the core engine. In that regard, the VPF acts as a protective layer for the core engine.
- As soon as the particles enter the fan stage, they interact with the reverse stream and adhere to it. This means that they move radially outward toward the shroud and are pushed out of the engine from the nacelle intake. Additionally, the particles are scattered after the interaction with the rotating VPF blades. Practical evidence for such behavior in general aviation propeller aircraft is also known to engineers.
- The effect of the fully coupled CFD-DPM approach is highlighted specifically in cases of particles with high C_D. These particles have a significant effect on the vortex location and size and thus FOI percentages are different. Therefore, it is recommended to use a coupled approach when a high concentration of high-C_D particles is present, while a decoupled approach, where the flow field solution is fixed, may be used for sparsely suspended particles.

- The effects of particle main parameters on the percentage of FOI have been investigated. The main FOI trend that is identified immediately is that fewer particles are ingested with an increase in their diameter. A change in density and/or C_D generates nonlinear relationships and a general conclusion is difficult to draw. Therefore, the nondimensional Stokes number is used to summarize all investigated FOI scenarios and determine general trends based on this parameter. The following trends are obtained:
  - At high Stokes numbers, the effect of particle density and irregularity follows an almost linear relationship. FOI percentages decrease with an increase in density, while the opposite happens with an increase in irregularity.
  - At low Stokes numbers, potential FOI levels can be determined based on the particle density. Moreover, linear boundaries that indicate expected FOI percentages based on the aircraft speed are identified. The linearity of these boundaries can be avoided by using data from additional simulations.

The findings from this paper in identifying and quantifying hitherto undescribed runway FOD ingestion into the engine address an important aspect of the operating envelope that includes the VPF operation at the end of the landing run. Consequently, the work provides important methodological methods and proposes trends on the expected FOI percentages that are necessary to explore the feasibility of using VPF as a thrust reverser for future, environmentally friendly aircraft.

Acknowledgment

Special thanks to Mr. Barry Moore and Mr. Rory Clarkson of Rolls-Royce plc. for comments and suggestions.

Funding Data

- Rolls-Royce plc (Funder ID: 10.13039/501100000767).

Nomenclature

A = surface area ratio
C = coefficient
F = force (N)
m = mass (kg)
N = rotational speed (% of max.)
t = time (s)
V = speed (m/s)
U = velocity (m/s)
x = position (m)

Subscripts and Superscripts

C = crosswind
D = drag
I = intake
L = landing
n = new particle position
p = particle property
R = rotation
shape = particle shape
sphere = spherical particles
0 = old particle position

Abbreviations

ADP = advanced ducted propulsor
DPM = discrete phase model
FOD = foreign object Debris
FOI = foreign object ingestion
GCI = grid convergence index
ISA, SL = international standard atmosphere, sea level
MTO = maximum take-off operating point
NACA = National Advisory Committee for Aeronautics
NPSS = numerical propulsion system simulation
OGV = outlet guide vane
QCSEE = quiet clean short-haul experimental engine
RANS = Reynolds-averaged Navier–Stokes
VPF = variable pitch fan

Appendix: Rotation Methods of Fan Blade Aerofoils

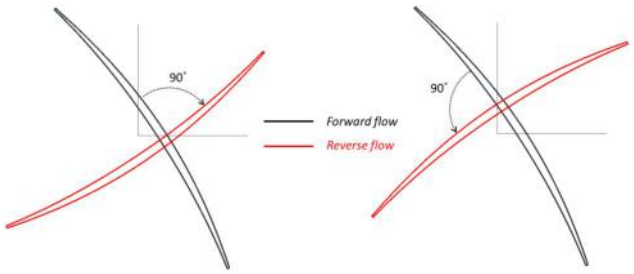

Fig. 14 Schematics showing clockwise (through feather pitch) and anticlockwise (through flat pitch) blade rotation [17]

References

[1] Mazzawy, R. S., ed., 2010, "Performance Study for the Benefits of a Variable Pitch Composite Fan," ASME Paper No. GT2010-22148.
[2] Krishnan, G., Perullo, C., and Mavris, D. N., 2013, "An Assessment of Relative Technology Benefits of a Variable Pitch Fan and Variable Area Nozzle," AIAA Paper No. 2013-3604.
[3] ASME, 1972, "Variable Pitch Ducted Fans for STOL Transport Aircraft," ASME Paper No. 72-GT-61.
[4] Halliwell, I., and Justice, K., 2012, "Fuel Burn Benefits of a Variable-Pitch Geared Fan Engine," AIAA Paper No. 2012-3912.
[5] McKay, B., "Next Generation Propulsion and Air Vehicle Considerations," AIAA 2009-4803.
[6] Levin, K., Rich, D., Ross, K., Franse, T., and Elliott, C., 2024, "Designing and Communicating Net-Zero Targets," World Resources Institute, Washington, DC, accessed Nov. 15, 2024, https://www.wri.org/research/designing-and-communicating-net-zero-targets
[7] Moore, R. D., Lewis, G. W., and Tysl, E. R., 1976, "Performance of a Low-Pressure Fan Stage With Reverse Flow," National Aeronautics and Space Administration, Scientific and Technical Information Branch, Cleveland, OH, Report No. NASA-TM-X-3349.
[8] Engineering, Advanced and Department, Technology Programs, 1975, "Quiet Clean Short-Haul Experimental Engine (QCSEE) Design Rationale," National Aeronautics and Space Administration, Scientific and Technical Information Branch, Washington, DC, Report No. NASA-CR-134842.
[9] Engineering, Advanced and Department, Technology Programs, "1977, Quiet Clean Short-Haul Experimental Engine (QCSEE)," National Aeronautics and Space Administration, Scientific and Technical Information Branch, Washington, DC, Report No. NASA-CR-135009.
[10] Levintan, R. M., 1975, "Q-Fan Demonstrator Engine," J. Aircr., **12**(8), pp. 658–663.
[11] Williams, T. S., and Hall, C. A., 2019, "Reverse Thrust Aerodynamics of Variable Pitch Fans," ASME J. Turbomach., **141**(8), p. 081008.
[12] Rajendran, D. J., Tunstall, R., and Pachidis, V., 2022, "Estimation of Resultant Airframe Forces for a Variable Pitch Fan Operating in Reverse Thrust Mode," ASME J. Eng. Gas Turbines Power, **144**(12), p. 121017.
[13] Rajendran, D. J., Tunstall, R., and Pachidis, V., 2021, "Flow Distortion Into the Core Engine for an Installed Variable Pitch Fan in Reverse Thrust Mode," ASME J. Turbomach., **143**(7), p. 071001.
[14] Rajendran, D. J., and Pachidis, V., 2019, "Fan Flow Field in an Installed Variable Pitch Fan Operating in Reverse Thrust for a Range of Aircraft Landing Speeds," ASME J. Eng. Gas Turbines Power, **141**(10), p. 101018.
[15] Rajendran, D. J., and Pachidis, V., 2021, "On the Use of an Inflatable Rubber Lip to Improve the Reverse Thrust Flow Field in a Variable Pitch Fan," ASME J. Eng. Gas Turbines Power, **143**(11), p. 111019.
[16] Vitlaris, D., Rajendran, D. J., Pachidis, V., Tunstall, R., and Whurr, J., 2024, "On the Flow Physics During the Transition of a Variable Pitch Fan From Nominal Operation to Reverse Thrust Mode," ASME J. Eng. Gas Turbines Power, **146**(4), p. 041001.
[17] Vitlaris, D., Rajendran, D. J., Tunstall, R., Whurr, J., and Pachidis, V., 2024, "On Hysteresis in a Variable Pitch Fan Transitioning to Reverse Thrust Mode and Back," ASME Paper No. GT2024-128701.
[18] Glenny, D. E., and Pyestock, N. G. T. E., 1968, "*Ingestion of Debris Into Intakes by Vortex Action*," Aeronautical Research Council, Great Britain, accessed Nov. 15, 2024, https://books.google.co.uk/books?id=-es-0AEACAAJ

[19] Robert, L., and Garret, F., 1955, "Ingestion of Foreign Objects Into Turbine Engines by Vortices," *National Aeronautics and Space Administration, Scientific and Technical Information Branch*, Cleveland, OH, Report No. NACA-TN 3330.
[20] McCreary, I., 2008, "The Economic Cost of FOD to Airlines," Insight SRI, Ltd., Washington, DC, https://fod-detection.com/wp-content/uploads/2009/12/the-economic-cost-of-fod.PDF
[21] Chauhan, T., Goyal, C., Kumari, D., and Thakur, A. K., 2020, "A Review on Foreign Object Debris/Damage (FOD) and Its Effects on Aviation Industry," Mater. Today: Proc., **33**, pp. 4336–4339.
[22] Menter, F. R., 1994, "Two-Equation Eddy-Viscosity Turbulence Models for Engineering Applications," AIAA J., **32**(8), pp. 1598–1605.
[23] Suzuki, M., Inaba, K., and Yamamoto, M., 2008, "Numerical Simulation of Sand Erosion in a Square-Section 90-Degree Bend," J. Fluid Sci. Technol., **3**(7), pp. 868–880.
[24] Schiller, L., 1933, "A Drag Coefficient Correlation," Zeit. Ver. Deutsch. Ing., **77**, pp. 318–320.
[25] Connolly, B. J., Loth, E., and Smith, C. F., 2020, "Shape and Drag of Irregular Angular Particles and Test Dust," Powder Technol., **363**, pp. 275–285.

https://dspace.org/

On runway foreign object ingestion with a variable pitch fan in reverse thrust mode

Vitlaris, Dimitrios; Rajendran, David John; Tunstall, Richard; Moore, Barry; Clarkson, Rory ...

2026-05
American Society of Mechanical Engineers (ASME)
https://doi.org/10.1115/1.4069791
Vitlaris D, Rajendran DJ, Tunstall R, et al., (2026) On runway foreign object ingestion with a variable pitch fan in reverse thrust mode. Journal of Engineering for Gas Turbines and Power, Volume 148, Issue 5, May 2026, Article number 051001

Downloaded from a DSpace repository. https://dspace.org/